Effects of smectite dehydration and illitisation on overpressures in sedimentary basins: A coupled chemical and thermo-hydro-mechanical modelling approach

Joachim Tremosa, Hélène Gailhanou, Christophe Chiaberge, Raymi Castilla, Eric Gaucher, Arnault Lassin, Claude Gout, Claire Fialips, Francis Claret

Effects of smectite dehydration and illitisation on overpressures in sedimentary basins: a coupled chemical and thermo-hydro-mechanical modelling approach

Joachim Tremosa[a,*], Helene Gailhanou[a], Christophe Chiaberge[a], Raymi Castilla[b], Eric C. Gaucher[b], Arnault Lassin[a], Claude Gout[b], Claire Fialips[b] and Francis Claret[a]

a BRGM, 3 av. Claude Guillemin, BP 36009, 45060 Orléans, France

b TOTAL S.A., Avenue Larribau, 64018 Pau, France

Corresponding author:

Joachim TREMOSA

BRGM, 3 av. Claude Guillemin BP6009

45060 Orléans, France.

* E-mail: j.tremosa@brgm.fr

Abstract

Diagenetic smectite dehydration and smectite-to-illite transition in clay-rich sediments can contribute to the generation of overpressure in sedimentary basins, because of the release of water associated with these mineralogical reactions. However, the challenge of deciphering the contribution of smectite dehydration and illitisation to fluid pressure amongst other mechanisms generating overpressure requires the different mechanisms at play to be jointly considered. Here, we developed a coupled chemical and thermo-hydro-mechanical code, named SURP, to calculate the overpressure generation in a sedimentary pile because of sediment compaction during its burial, temperature increase, water flow and because of the release of water by clay dehydration and illitisation. For this purpose, a revised thermodynamic model describing smectite dehydration by a solid solution approach was considered, together with the different thermo-hydro-mechanical processes occurring in sedimentary basins. The SURP code was applied to the case study of an overpressured passive margin in the Niger Delta, composed of thick shale layers in a sedimentary pile. In this geological scenario, smectite dehydration was simulated and could explain 10 to 30 % (20 to 50 bar) of the present day overpressure in the main reservoirs, in addition to compaction disequilibrium.

Keywords: overpressure; smectite; dehydration; fluid generation; fluid pressure; THMC; Niger Delta

1. Introduction

Overpressures, or abnormal fluid pressures, are frequently encountered in sedimentary basins and consist in fluid pressures exceeding the hydrostatic head. During the drilling of deep reservoirs, it is necessary to anticipate and to be able to control the fluid pressure conditions for ensuring well integrity and safety. Understanding the fluid pressure regime is also useful for evaluating fluid and hydrocarbon migration and trapping over the sedimentary basin history. The water flushing of hydrocarbons linked to overpressures can clearly be a cause of unsuccessful results during exploration phases.

These overpressures generally correspond to a delay in the expulsion of the fluids contained in the porosity and can be caused by different mechanisms (Neuzil, 1995; Swarbrick and Osborne, 1998), including: i) mechanical compaction disequilibrium; ii) tectonic compression; iii) mineralogical transformations releasing water; iv) hydrocarbon generation; or v) osmotic processes. Combinations of several of these mechanisms are frequently the cause of the abnormal pressure profile in a sedimentary pile and, for interpreting or predicting overpressure, it is necessary to distinguish the respective contribution of each mechanism. For this purpose, the use of basin models able to calculate the pressure evolution in the sedimentary pile by taking into account the different mechanisms generating overpressures is a pertinent approach (Swarbrick and Osborne, 1998; Wangen, 2001; Nordgård Bolås et al., 2004; Tremosa et al., 2012).

Overpressures linked to the presence of clay layers are not always correctly interpreted. We have to distinguish (i) the water produced by mechanical compaction and from the macroporosity of the clay formations and (ii) the water produced by the thermodynamic transformation of the clay minerals (Figure 1). By thermodynamic transformation, we mean the dehydration of smectite and the illitisation processes of hydrated smectite. Several cases of overpressures generated by clay dehydration are reported in the literature (Bruce, 1984; Shaw and Primmer, 1989; Kooi, 1997; Gordon and Flemings, 1998; Nordgård Bolås et al., 2004; Tanikawa et al., 2008), as an additional mechanism to compaction disequilibrium. However, clay dehydration is ruled out in most studies on the origin of overpressures

64 and is only considered as one unloading process amongst others that decreases the effective stress
65 without changing the porosity. Clay dehydration is rarely considered in forward modelling of
66 overpressure build-up but some models have done so, suggesting that clay dehydration can contribute
67 up to ⅓ of the overpressure, depending on the geological scenario (Audet, 1995; Wangen, 2001).
68 When smectite dehydration and illitisation were considered in a pressure or transport calculation
69 model in a sedimentary basin (Audet, 1995; Wangen, 2001; Saffer and McKiernan, 2009), the
70 mineralogical process releasing water was simplified, only describing a continuous release of water
71 depending on temperature but without considering thermodynamic constraints and dehydration steps.
72 Conversely, when a thermodynamic model was established and used to correctly describe clay
73 dehydration, the coupling with the pressure calculation was partial (Colten-Bradley, 1987; Meiller,
74 2013). In these last models, the pressure corresponding to the volume of released water was added to
75 the calculated pressure, thus accounting for compaction but without considering the feedback of this
76 additional pressure excess on flow and effective stress.
77 In this paper, we are presenting a model, called SURP, for pore pressure calculation during the burial
78 of a sedimentary pile, accounting for water flow, compaction, temperature increase and involving an
79 advanced thermodynamic model describing smectite dehydration (Vidal and Dubacq, 2009). Hence,
80 pore pressure is calculated by considering both the different thermo-hydro-mechanical processes
81 occurring in a sedimentary basin and the release of water by smectite, calculated depending on the
82 modelled temperature and pressure evolution. A coupled approach considering a sound description of
83 clay dehydration in pore pressure calculation was missing to evaluate the influence of smectite
84 dehydration on overpressure generation. The developed model was applied to a case study in the Niger
85 Delta, where the influence of water released by thick shale layers on overpressure is discussed.
86

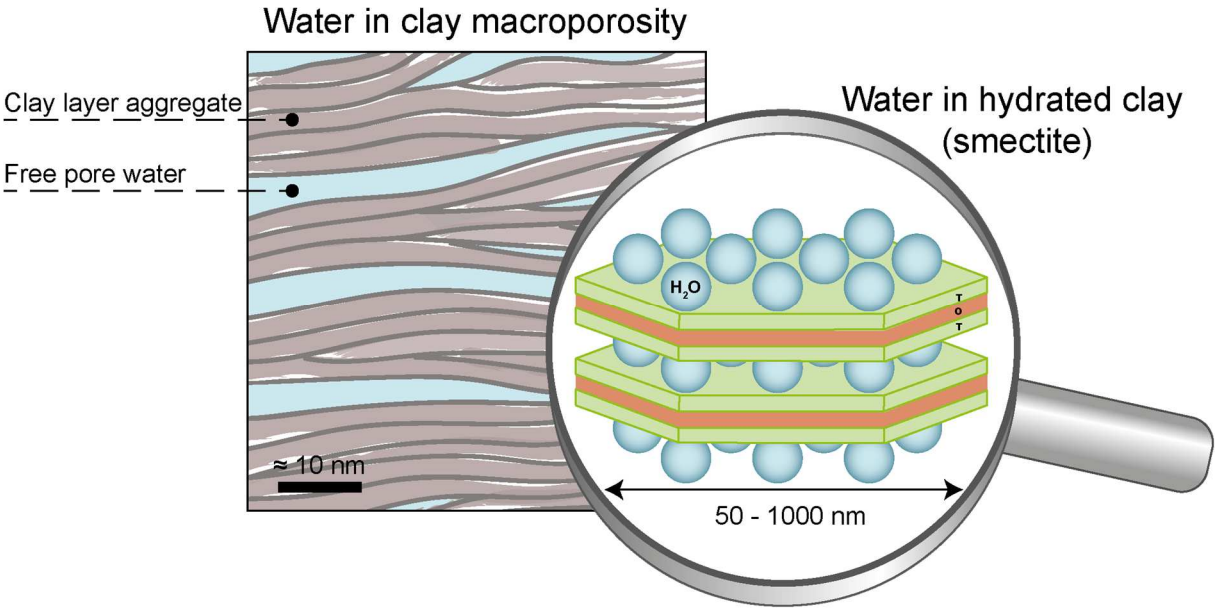

Figure 1. Schematic view of the distribution of water in a clay-rock: in the macroporosity between clay aggregates and in the interlayer space between clay crystallite.

2. Model development for overpressure calculations during burial diagenesis of marine sediments

2.1. Objective of the SURP code

The SURP code has been developed to account for both thermo-hydro-mechanical and mineralogical effects and their reciprocal influence, including the influence of temperature and pressure evolution on clay dehydration and the influence of the water released by mineralogical reactions on the flow, the fluid pressure and the effective stress in the sedimentary pile. In the SURP coupling approach, the thermo-hydro-mechanical calculations are made using a Python code source that can be coupled through a sequential non-iterative approach with the IPHREEQC geochemical calculation code (Charlton and Parkhurst, 2011) used to carry out the thermodynamic and mineralogical calculations.

Hence, the aim of the SURP code is to evaluate the effect of water releases by smectite mineralogical transformations on the pore pressure in a sedimentary pile and in particular in clayey layers. The geological context of application corresponds to a passive margin in the marine domain, where the clay layer of interest is buried over time because of the deposition of overlying sediments. The principle of the pore pressure calculation consists in considering the following processes in a 1D sedimentary pile over time:

- Sediment deposition;
- Burial and compaction due to overlying sediments giving rise to a porosity reduction and a decrease of the sediment thickness;
- Temperature increase with depth;
- Water release during clay mineral transformations;
- Modification of the thermal, hydraulic and mechanical properties of the rock during the burial;
- Water flow in the sedimentary pile and possible overpressure build-up.

2.2. Thermodynamic model for dehydration of smectites

A thermodynamic model was implemented in the SURP code in order to assess the amount of water released by the dehydration of smectites occurring during the burial of sediments. The proposed thermodynamic approach, based on solid solution models, aims to describe the thermodynamic properties of the smectite mineral as well as the amount of hydration water bound to the smectite, i.e. interlayer water, as a function of temperature, pressure and water activity. It was adapted from the model from Vidal and Dubacq (2009) established to simulate the dehydration of dioctahedral Al-smectites and the smectite-to-illite conversion occurring with increasing temperature and pressure and decreasing water activity.

2.2.1. Dehydration model from Vidal and Dubacq (2009)

According to the Vidal and Dubacq (2009) model, the compositional and interlayer charge variations of dioctahedral smectite and illite can be described by non-ideal solid solutions using three end-members, namely hydrated beidellite (Beid.m_nH$_2$O) $R^+_{0.3}[Al_2]^{VI}[Al_{0.3}Si_{3.7}]^{IV}O_{10}(OH)_2$,$m_nH_2$O, dehydrated beidellite (Beid.A) $R^+_{0.3}[Al_2]^{VI}[Al_{0.3}Si_{3.7}]^{IV}O_{10}(OH)_2$, and anhydrous R^+-mica ($R^+[Al_2]^{VI}[AlSi_3]^{IV}O_{10}(OH)_2$, with R^+ = K^+, Na^+, $0.5Ca^{2+}$, or $0.5Mg^{2+}$). Four solid solutions were defined, with four hydrated beidellite end-members at m_0 = 0.7, m_1 = 2, m_2 = 4 and m_3 = 7 H$_2$O/O$_{10}$(OH)$_2$, for the beidellite end-members at 0, 1, 2 and 3 water layers, respectively. Besides, the amounts of interlayer water in the hydrated beidellite end-members were assumed not to depend on the nature of the interlayer cation. Therefore, considering a dioctahedral smectite with an intermediary

composition between beidellite and R^+-mica , the Vidal and Dubacq (2009) model can predict the most stable solid solution amongst the four solid solutions Beid.A-Beid.$m_n$$H_2O$-Mica, at fixed pressure, temperature and water activity. The transition between smectite with *n* and (*n*-1) layers occurs at fixed temperature and water activity, with the simultaneous attainment of the following equilibria:

$$Smect.m_{(n-1)}H_2O = Smect.A + m_{(n-1)}\,H_2O \qquad \textbf{eq. 1}$$

$$Smect.m_nH_2O = Smect.A + m_n\,H_2O \qquad \textbf{eq. 2}$$

$$Smect.m_nH_2O = Smect.m_{(n-1)}H_2O + (m_n\text{-}m_{(n-1)})\,H_2O \qquad \textbf{eq. 3}$$

Such a transition generates a sudden release of water, calculated from the conditions of equilibrium (eq. 1 to 3). It results in a stepwise dehydration of smectite at each transition temperature. Besides, inside the stability domain of a given solid solution, the variations of volume and water amount are continuous, as described by the thermodynamic parameters of the non-ideal solid solution.

In our approach, the model from Vidal and Dubacq (2009) was not directly applicable for two main reasons: (i) it is currently non-feasible to introduce non-ideal parameters for ternary solid solutions in the IPHREEQC code (Charlton and Parkhurst, 2011) used for geochemical calculations in the SURP code, and (ii) the compositional range of dioctahedral smectite is restricted to Si^{4+}, Al^{3+} and interlayer R^+ (K^+, Na^+, $Ca^{2+}/2$ or $Mg^{2+}/2$) cations. Despite the model having been extended to (Al, Mg, Fe) octahedral compositions of dioctahedral smectites by Dubacq et al. (2010), it required the use of non-ideal quaternary solid solutions, not compatible with the IPHREEQC code. Nevertheless, we adapted the model from Vidal and Dubacq (2009), by applying a similar methodology based on the use of solid solutions with hydrated smectite end-members and dehydrated smectite, but restricted to binary solid solutions and to a fixed smectite composition, assumed to be representative of the studied geological system.

2.2.2. The smectite dehydration model in the SURP code

In the present approach, we consider a montmorillonite composition for smectite instead of a beidellite composition because in natural diagenetic environments, the smectitic components in interstratified

158 illite-smectite are mostly reported to be of the montmorillonite type (Velde and Brusewitz, 1986;
159 Meunier and Velde, 1989; Srodon et al., 2009). Illite-beidellite mixed layers are less frequently
160 observed and generally associated with hydrothermal conditions.

161 The montmorillonite composition departs from the compositional ranges used in the Vidal and Dubacq
162 (2009) model, by its charge deficit located in the octahedral layer instead of the tetrahedral layer, due
163 to the concomitant presence of Al and Mg in octahedral sites. However, the approach used by the
164 authors for extracting the amounts of interlayer water and the energies of hydration as a function of the
165 water activity was based on experimental data obtained for montmorillonites, with interlayer charges
166 at ~ 0.35 – 0.38 eq/$O_{10}(OH)_2$ (Ferrage et al., 2005). For this reason, the hydration parameters were
167 similar to those used in the Vidal and Dubacq (2009) model for hydrated beidellite end-members.
168 Finally, our model was using three binary solid solutions between the hydrated montmorillonite end-
169 member and the dehydrated end-member. The hydrated components, Mnt_Na.3w (3 water layers),
170 Mnt_Na.2w (2 water layers) and Mnt_Na.1w (1 water layer), contain respectively $m_3 = 7$, $m_2 = 4$ and
171 $m_1 = 2$ $H_2O/O_{10}(OH)_2$.

172 The thermodynamic properties of the dehydrated montmorillonite ($\Delta H_f°$, $S°$, $V_m°$, $C_p(T)$) were
173 estimated using the set of predicting models from Blanc et al. (2015). These models for enthalpy,
174 entropy, molar volume and heat capacity function were all calibrated using a common and consistent
175 thermodynamic dataset, based on a rigorous selection between experimental data from the literature
176 and associated exclusively with phyllosilicates. This recent work provides a consistent dataset for
177 smectites and was thus preferred to the approach used by Vidal and Dubacq (2009), which combined
178 different methods for enthalpy, entropy and heat capacity function.

179 Estimation of the thermodynamic dataset for the hydrated end-members was performed according to
180 the procedure described by Vidal and Dubacq (2009), except for molar volumes. The thermodynamic
181 parameters ($\Delta H_f° m_n H_2O$, $S°H_2O_{(i)}$, $C_p(T)$) associated with interlayer water for Na-montmorillonite end-
182 members are the same as those used by Vidal and Dubacq (2009) for Na-beidellite end-members
183 (Table 1). The molar volumes $V_m°$ of hydrated montmorillonites at n water layers (n = 1, 2, 3) were
184 estimated using the recent advances from Meiller (2013). The author established functions to express

185 the dependency of the molar volume on the number of water layers, the nature of the interlayer cation
186 (Na and Ca) and the substitution rate Al-Mg in the octahedral sites of the smectite.

187 The non-ideality of the solid solutions is described by the same Margules parameters as those used in
188 the Vidal and Dubacq (2009) model, extracted from the Ransom and Helgeson (1994) model. Their
189 values were assumed at W = -10 kJ for Smect.m_nH$_2$O – Smect.A (n = 1, 2 or 3 water layers) in the case
190 of dioctahedral smectites.

191 Finally, the thermodynamic dataset used for the solid-solution models is reported in Table 1 and Table
192 2, in the case of the low-charge montmorillonite $Na_{0.33}Si_4(Al_{1.67}Mg_{0.33})O_{10}(OH)_2$ (Mnt_Na).

193

194 *Table 1. Standard-state thermodynamic properties of the montmorillonite end-members.*

	$m_n H_2O$ (mol/$O_{10}(OH)_2$)	$\Delta G_f°$ (kJ/mol)	$\Delta H_f°$ (kJ/mol)	$S°$ (J/mol/K)	$V°$ (cm3/mol)	A	B	C	$\Delta H_f° m_n H_2O$ (kJ)
Mnt_Na.A	0	-5320.51*	-5688.74*	276.76*	133.83*	330.7*	225.94*	-78.055*	
Mnt_Na.1w	2	-5806.02	-6280.54	386.76	170.53	419.37	275.26	-91.74	293.85
Mnt_Na.2w	4	-6283.23	-6864.04	496.76	207.13	508.05	324.58	-105.43	291.75
Mnt_Na.3w	7	-6994.77	-7735.03	661.76	258.63	641.06	398.56	-125.96	290.33

Notes: The $C_p(T)$ functions of the clay minerals are expressed by $C_p(T) = A + 10^{-3}\ B\ T + 10^5\ C\ T^{-2}$, where A, B and C are Maier-Kelley coefficients.
(*) estimated from Blanc et al. (2015) model
The properties of interlayer water, $\Delta H_f° m_n H_2O = (H_f°\text{Mnt}.m_n H_2O - H_f°\text{Mnt}.m_{(n-1)} H_2O)/(m_n - m_{(n-1)})$, $C_p(T)$ function and entropy $S°H_2O_{(i)} = 55$ J/mol/K are given by Vidal and Dubacq (2009).
The molar volumes of hydrated end-members are calculated according to Meiller (2013).

195

196

197

198

199

200 *Table 2. Temperature dependency of the equilibrium constant for the reaction of dissolution of the montmorillonite end-members.*

	log*K*	A_1	A_2	A_3	A_4	A_5	Reaction of dissolution
Mnt_Na.A	3.31	-1.1860978E+03	-2.0559084E-01	6.2330921E+04	4.3249803E+02	-2.5368937E+06	$Na_{0.33}Mg_{0.33}Al_{1.67}Si_4O_{10}(OH)_2 + 6H^+ + 4H_2O = 1.67Al^{+++} + 0.33Mg^{++} + 0.33Na^+ + 4H_4SiO_4$
Mnt_Na.1w	1.35	-1.1353999E+03	-1.9610007E-01	5.8199874E+04	4.1458388E+02	-2.2979605E+06	$Na_{0.33}Mg_{0.33}Al_{1.67}Si_4O_{10}(OH)_2{:}2H_2O + 6H^+ + 2H_2O = 1.67Al^{+++} + 0.33Mg^{++} + 0.33Na^+ + 4H_4SiO_4$
Mnt_Na.2w	0.83	-1.0826594E+03	-1.8627762E-01	5.4396671E+04	3.9592168E+02	-2.0533067E+06	$Na_{0.33}Mg_{0.33}Al_{1.67}Si_4O_{10}(OH)_2{:}4H_2O + 6H^+ = 1.67Al^{+++} + 0.33Mg^{++} + 0.33Na^+ + 4H_4SiO_4$
Mnt_Na.3w	0.81	-1.0149545E+03	-1.7339608E-01	4.9505162E+04	3.7210547E+02	-1.7182698E+06	$Na_{0.33}Mg_{0.33}Al_{1.67}Si_4O_{10}(OH)_2{:}7H_2O + 6H^+ = 1.67Al^{+++} + 0.33Mg^{++} + 0.33Na^+ + 4H_4SiO_4 + 3H_2O$

Note: $\log K = A_1 + A_2\,T + A_3/T + A_4*\log(T) + A_5/T^2$

log*K* and A_1-A_5 parameters were calculated using the thermodynamic properties of aqueous species selected from the Thermoddem database (Blanc et al., 2012).

201

2.2.3. Verification of the consistency of the thermodynamic data for dehydrated and hydrated Na-Montmorillonite

The consistency of the thermodynamic data for the dehydrated and hydrated Mnt_Na end-members was first assessed by calculating the dehydration isotherm of the smectite at 25 °C and 1 bar pressure, using PHREEQC v3 (Parkhurst and Appelo, 2013) and the Thermoddem database (Blanc et al., 2012) (Figure 1).

The comparison with the stepwise dehydration isotherm is very consistent with the previous results obtained by Vidal and Dubacq (2009) for Na-beidellite (Figure 2). These results are in reasonable agreement with the experimentally determined basal spacing (not shown here) and hydration isotherms, despite some differences due to the coexistence of smectites with different hydration states in the experimental isotherms, as discussed in Vidal and Dubacq (2009).

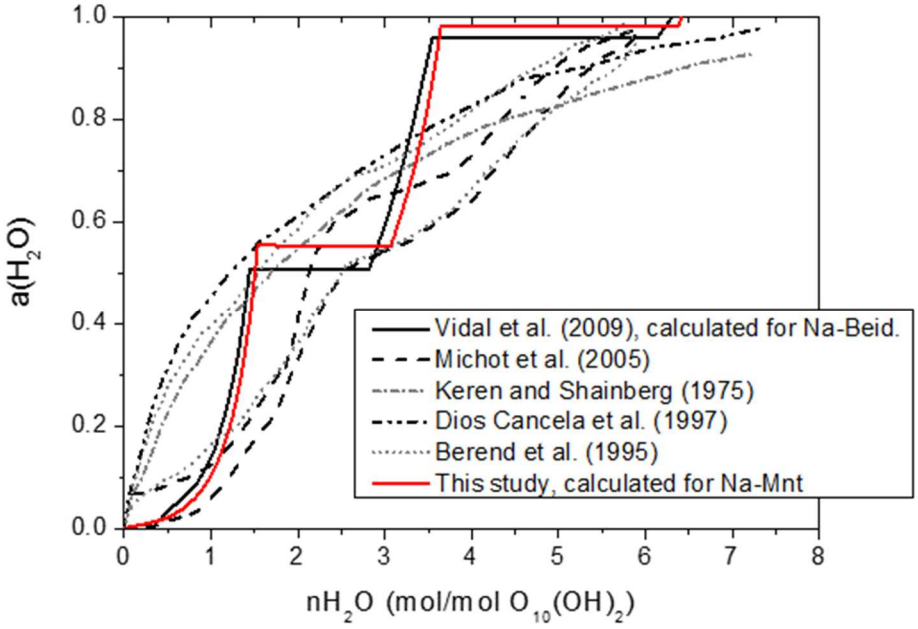

Figure 2. Comparison of measured dehydration isotherms for smectite with results from the Vidal and Dubacq (2009) *model and its adaptation for the Na-Montmorillonite.*

A second verification was performed by calculating a phase diagram for the Na_2O-K_2O-SiO_2-Al_2O_3-MgO-H_2O system (Figure *3*), using the Geochemist's Workbench® software, at the saturation vapour

pressure. The results indicated that all smectite end-members (Mnt_Na.A, 1w, 2w, 3w) exhibit a stability domain depending on the temperature region, in which the corresponding solid solution is predominant. Moreover, the transition temperatures between the stability domains of the smectite end-members are consistent with those previously calculated by Vidal and Dubacq (2009) for Na-beidellite. This figure also highlights the expected behaviour of illite, the stability domain of which develops as the potassium concentration increases, and further enlarges at elevated temperatures.

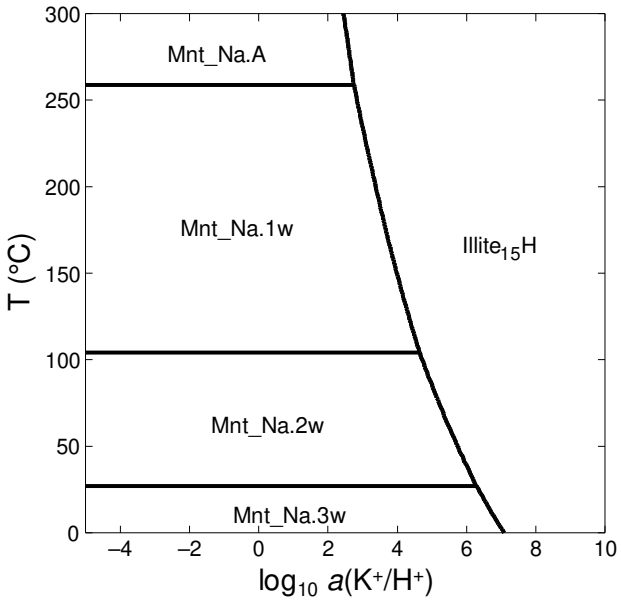

Figure 3. Composition-temperature phase diagram calculated for the Na_2O-K_2O-SiO_2-Al_2O_3-MgO-H_2O system ($Illite_{15}H = K_{0.85}Si_{3.7}Al_{0.3}(Al_{1.85}Mg_{0.15})O_{10}(OH)_2$). The activities of Na, H_4SiO_4, Al and Mg in solution are constrained by equilibrium reactions with minerals analcime, quartz, kaolinite and antigorite, respectively.

2.2.4. Stability domains of solid solutions as a function of temperature and pressure

In order to take into account the effect of pressure on the stability domains of the solid solutions, the variation of the transition temperatures for the smectite end-members with pressure were calculated using the PHREEQC code. In the case of the montmorillonite Mnt_Na, the dependency of the transition temperatures on pressure is low and may be described by using linear functions (Table 3).

Table 3. Limits of the stability domains as a function of temperature and pressure.

Transition	Linear function
SS3w – SS2w	$P_{tr} = 115.84*T_{tr} - 3304.9$ ($R^2 = 0.9716$)
SS2w – SS1w	$P_{tr} = -67.021*T_{tr} + 6941$ ($R^2 = 0.9955$)

Notes: P expressed in bar, T in °C.
SSnw means the solid solution Mnt_Na.nw-Mnt_Na.A

2.3. Smectite-to-illite conversion model

Smectite illitisation is widely described in the literature, notably in the case of burial diagenesis of clay-rich sediments (Weaver, 1959; Burst, 1969; Perry and Hower, 1970; Altaner and Ylagan, 1997; Lanson et al., 2009). The transformation process generates the formation of intermediate I/S phases, with illite content progressively increasing with temperature, the concentration of potassium in pore water, the water/rock ratio and geological time (Altaner and Ylagan, 1997). In the early stage of burial diagenesis, discrete smectite and randomly interstratified I/S coexist, with a progressive increase in illite content in the I/S. When the latter is higher than ~ 50% of illite (Inoue et al., 1987), short-range ordered (R1) interstratified I/S are observed. Lanson et al. (2009) showed notably from structural characterization of Texas Gulf Coast interstratified series that intermediate I/S phases and I/S/Chlorite phases may coexist. For the most illite-rich contents (> 85% illite), long-range ordered interstratified I/S ($R \geq 3$) are observed (Inoue et al., 1987).

Several kinetic models have been developed in order to describe the smectite-to-illite transformations during burial diagenesis in sedimentary basins (Altaner, 1989; Pytte and Reynolds, 1989; Velde and Vasseur, 1992; Cuadros, 2006). Among these models, that of Cuadros (2006) takes better account of the question of the availability of potassium for the smectite-to-illite reaction. Indeed, K concentration is the most problematic variable in the modelling of smectite illitisation kinetics, since it is affected by the competition with other exchangeable cations, also dependent on the degree of hydration of the smectite interlayers. The model from Cuadros (2006) involves the "effective K concentration" variable, which differs from the actual K concentration by integrating notably cationic exchange in smectitic interlayers.

Such a kinetic model cannot be easily implemented in our modelling approach based on water/rock thermodynamic equilibrium considerations since it would require the thermodynamic parameters associated with discrete I/S series to be determined and the dehydration of smectite layers with burial depth to be taken into account. Finally, for the sake of simplicity, it is assumed that the smectite-to-illite conversion does not involve the formation of interstratified I/S and can be roughly described by the simplified reaction:

$$\text{Mnt\_Na} + K^+ + Al^{3+} = \text{illite} + \text{quartz} + H_2O \qquad \textbf{eq. 4}$$

This equation is not balanced but simply aims to indicate that the smectite-to-illite transformation as described in our model requires a source of potassium and aluminium and generates quartz. This approach is consistent with the implementation of the dehydration model for montmorillonite Mnt_Na.

2.4. Thermo-hydro-mechanical model including chemical forcing

2.4.1. Water flow model

The pore pressure evolution in a porous media is calculated using the continuity equation which describes the mass conservation in a given volume. Its general expression giving the variation over time of the mass of water in a volume of saturated poroelastic media, accounting for a source term, is expressed by (De Marsily, 1986; Ingebritsen et al., 2006):

$$\frac{\partial(n\,\rho_f)}{\partial t} = \nabla\left[\frac{k\,\rho_f}{\mu_f}\left(\nabla P - \rho_f g \nabla z\right)\right] + \Gamma \qquad \textbf{eq. 5}$$

where, n is the porosity, ρ_f is the fluid density (kg.m^{-3}), k is the intrinsic permeability (m^2), μ_f is the fluid dynamic viscosity (Pa.s), P is the pore pressure (Pa), g is the acceleration constant due to gravity (9.81 m.s^{-2}), ∇z is (0,0,1) if the z axis is orientated downward and Γ is a source term corresponding to input or withdrawal of water in the porosity. In the present case, this source term corresponds to the water released by smectite dehydration and by smectite transformation to illite.

The continuity equation can be written in such a way that the variation of fluid mass can be dependent on the variations over time of pore pressure, mechanical stress and temperature. This expression of thermo-hydro-mechanical coupling including a vertical load stress which can vary over time can be written as follows (Ingebritsen et al., 2006):

$$Ss'\frac{\partial P}{\partial t} - Ss'\xi\frac{d\sigma_{zz}}{dt} - \rho_f g \Lambda'\frac{\partial T}{\partial t} = \nabla\left[g\frac{k\,\rho_f}{\mu_f}\left(\nabla P - \rho_f g \nabla z\right)\right] + \Gamma \qquad \textbf{eq. 6}$$

In this expression, Ss' is the unidimensional specific storage coefficient (m^{-1}), ξ is an unidimensional loading coefficient (dimensionless), σ_{zz} is the total vertical stress (Pa), Λ' is the thermal response coefficient ($°C^{-1}$) and T is the temperature (°C).

The unidimensional specific storage coefficient is expressed by (Van Der Kamp and Gale, 1983):

$$Ss' = \rho_f g\left[(c_b - c_s)(1-\lambda) + \left(nc_f - nc_s\right)\right] \qquad \textbf{eq. 7}$$

The unidimensional loading coefficient is defined as:

$$\xi = \frac{B(1+\nu)}{3(1-\nu) - 2\alpha B(1-2\nu)} \qquad \textbf{eq. 8}$$

with:

$$\lambda = \frac{2\alpha(1-2\nu)}{3(1-\nu)} \qquad \textbf{eq. 9}$$

where, c_f, c_b and c_s, are the compressibilities (Pa^{-1}) of fluid, porous media and solid, respectively, B is the Skempton coefficient (dimensionless), ν the Poisson's ratio (dimensionless) and α is the Biot coefficient (dimensionless).

Skempton and Biot coefficients can be expressed as a function of the compressibilities of fluid, porous media and solid. Thus:

$$B = \frac{c_b - c_s}{(c_b - c_s) + n\left(c_f - c_s\right)} \qquad \textbf{eq. 10}$$

and:

$$\alpha = 1 - \frac{c_s}{c_b} \qquad \textbf{eq. 11}$$

The compressibilities of fluid, porous media and solid can be expressed as a function of the Young modulus E (Pa), a parameter dependent on the material:

$$c_b = \frac{3(1-2\nu)}{E} \qquad \textbf{eq. 12}$$

$$c_s = \frac{(1-2\nu)(1+\nu)}{E(1-\nu)} \qquad \textbf{eq. 13}$$

To solve the flow equation (**eq. 6**), it is then necessary to determine the different coefficients involved, which can be written as a function of properties of the fluid, the solid and the porous media (Supplementary material A). It is also necessary to calculate the variation over time of the mechanical stress and of the temperature in the considered volume. The vertical mechanical stress is calculated from the weight of the sediments overlying the considered point, as follows:

$$\sigma_{zz} = \int_0^z \rho_b g dz \qquad \textbf{eq. 14}$$

where, ρ_b is the porous media density, obtained from the porosity and the fluid and solid densities: $\rho_b = \rho_s(1-n) + \rho_f n$; or directly from a density well log.

Temperature is obtained from the depth and the geothermal gradient (G_T in °C.m^{-1}). Hence, sediment temperature increases over time with sediment burial. Temperature is calculated as follows:

$$T = G_T z \qquad \textbf{eq. 15}$$

The source term for the input or withdrawal of water Γ (kg.m^{-3}.s^{-1}) in the continuity equation (**eq. 6**) corresponds to a mass of water produced or extracted in the porosity for a given volume and for a given length of time. Since the thermo-hydro-mechanical calculation is made for a 1D geometry, there is no notion of volume. The mass of water liberated or consumed by mineralogical reactions and calculated using IPHREEQC for 1kg of water (by convention) is then converted to m^3 of porous media, in order to respect the mass balance in the pressure calculation. The balance of the water released and consumed by mineralogical reactions that needs to be respected between Python and IPHREEQC can thus be written as follows:

$$\Gamma = \frac{d}{dt}(solution\_volume) \times \rho_f \times n \qquad \textbf{eq. 16}$$

where, dt is the time step length (s). The solution density ρ_f is calculated by IPHREEQC depending on its chemical composition and the temperature and pressure conditions.

2.4.2. Compaction model

During their burial in a sedimentary basin, sediments experience compaction because of the deposition of overlying sediments. Compaction is a deformation mechanism which gives rise to a reduction of the

porosity. In a basin model, this reduction of porosity is calculated using relationships introducing a dependence on the depth (e.g. Athy's law) or using relationships calculating the porosity as a function of the effective stress undergone by the rock. The latter kind of expressions allows the driving mechanism of porosity reduction, i.e., the effective stress, to be taken into account. One of these expressions which was shown to provide interesting results (Lambe and Whitman, 1979; Burland, 1990; Nygård et al., 2004) is used in the present work:

$$e = e_0 - C_c log\left(\frac{{\sigma_{zz}}'}{{\sigma_{zz\,0}}'}\right) \qquad \textbf{eq. 17}$$

where, e is the void ratio (dimensionless), linked to porosity by the relation $e = n/(1-n)$, C_c is the compaction index (dimensionless) and ${\sigma_{zz}}'$ is the vertical effective stress (Pa). e_0 is the void ratio for the reference value of vertical effective stress ${\sigma_{zz\,0}}'$. This reference value corresponds to the consolidation limit of the rock and is considered equal to 1 MPa in the calculations. The rock has an elastic behaviour for effective stress lower than this limit and has a plastic behaviour for effective stress values higher than this consolidation limit. In this case the deformation undergone by the rock is irreversible. This porosity model dependent on the effective stress can be used in the present calculations because the weight of the sediments and the pore pressure are known.

As a consequence of the compaction of the rock and of the associated porosity reduction, the thickness of each lithological level and of each cell in the numerical model diminishes. The collapse of the cells is considered to be instantaneous (no time effect on deformation such as creep or stress relaxation) and the hypothesis is made that the solid is incompressible. The thickness diminution is thus only dependent on the loss of porosity. The new cell thickness is calculated by the balance between the initial thickness and porosity and the new porosity after compaction.

The effective stress necessary to calculate the porosity reduction by compaction (**eq. 17**) is calculated as follows:

$$\sigma'_{zz} = \sigma_{zz} - \alpha\, P \qquad \textbf{eq. 18}$$

Biot's equation is preferred to Terzaghi's original equation to calculate the effective stress because it has been shown that using a Biot coefficient of 1 (or no Biot coefficient) gives overestimated porosity

reductions in overpressured areas (Burrus, 1998). In addition, the Biot coefficient actually varies with porosity and becomes lower than 1 when porosity decreases (Supplementary material A).

2.5. IPHREEQC-Python coupling

One of the main goals of the SURP code is to jointly consider thermo-hydro-mechanical evolution and mineralogical transformations in the geological system under study. Hence, calculation of the chemical reactions has to consider the thermo-hydro-mechanical evolution of the system and, inversely, thermo-hydro-mechanical calculation needs to take into account the effect of the chemical reactions. In this way, a sequential non-iterative approach has been implemented whereby the thermo-hydro-mechanical model is solved numerically using Python v 2.7 language and the chemical and mineralogical reactions are calculated with IPHREEQC. At each time step, the reactive calculations using IPHREEQC are launched from Python as a DLL dynamic library, using updated parameters as a function of pressure, temperature and porosity evolution on the sedimentary pile. Once the IPHREEQC calculations have been made, the mineralogical evolution, the balance of water produced and consumed by the minerals and the solution density are entered into the thermo-hydro-mechanical calculations in Python. The architecture of these coupled calculations is schematised in Figure 4, where the successive calculations and parameters updating during one time-step are shown. Each time step gives rise to the numerical resolution of the pore pressure in the sedimentary sequence and allows the resulting overpressure to be calculated.

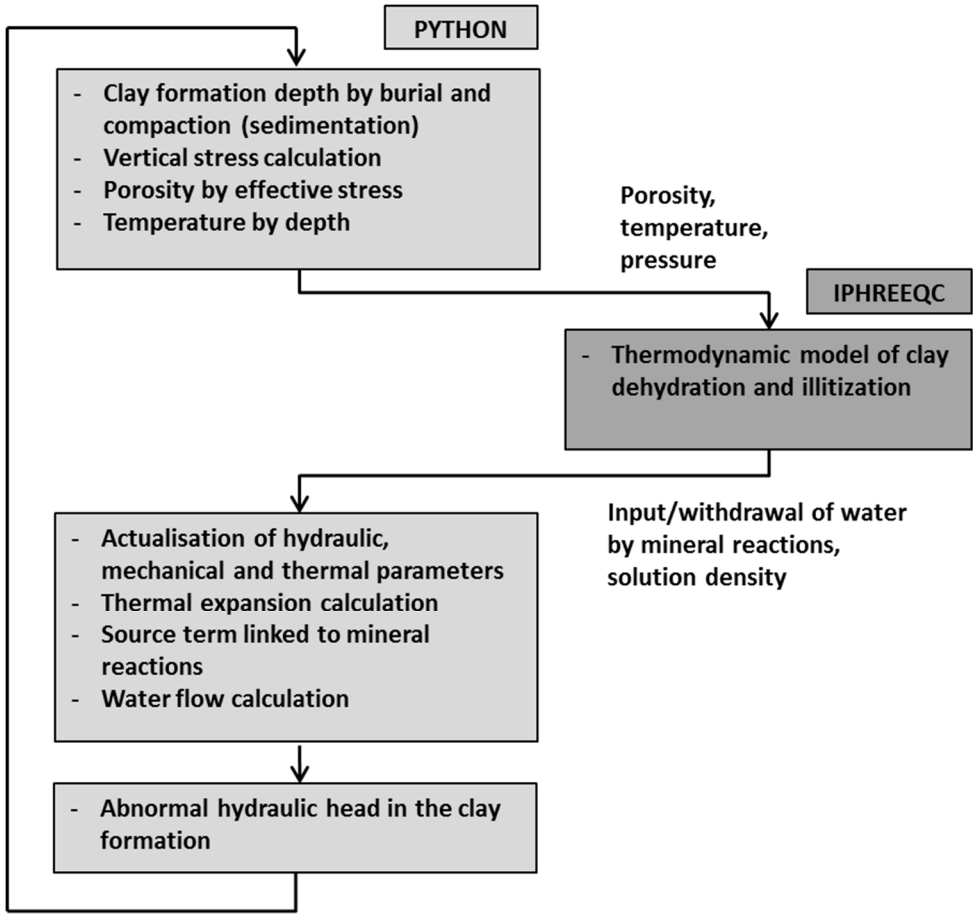

Figure 4. Architecture of the calculations made during one time step by the SURP code, including the coupling of the thermo-hydro-mechanical calculations with Python language and the thermodynamic reactive calculations made using the IPHREEQC code.

3. Effect of clay mineralogical reactions on overpressures in Niger Delta

In order to evaluate the influence of smectite dehydration and illitisation effects on overpressure, the SURP code was applied to a pore pressure calculation in the case of the Niger Delta. An overpressure has been reported in this area, which is formed of thick shale layers and where the geothermal gradient is normal. It appeared preferable to apply the SURP code to a real geological context than to limit its application to generic scenarii because the pore pressure that can be calculated with such a model is highly dependent on the sedimentary pile geometry, the sedimentation rate or the temperature evolution (Audet, 1995; Wangen, 2001).

3.1. Geological context of the Niger Delta

In the Niger Delta, the Akata, Agbada and Benin formations have been successively depositing since the Tertiary during various prograding megasequences in the Gulf of Guinea (Whiteman, 1982;

Chukwu, 1991). The Akata formation is the basis of deltaic deposits and is formed of thick clay deposits (up to 7000 m thick) which act as the primary source of hydrocarbons in the Niger Delta. The Agbada formation has been depositing since the Eocene and presents alternations of claystone and sandstone layers over 4000 m thick. Most of the hydrocarbon reservoirs are located in the Agbada formation. The Benin formation is the youngest one and is formed of alluvial and shoreline sand deposits.

The Niger Delta was identified for a long time as being an area presenting overpressures in particular in the deepest parts (Akata Fm). By applying the equivalent depth method on onshore and offshore wells of the Niger Delta, Owolabi et al. (1990) estimated that compaction disequilibrium is the main cause of overpressures. By using 3D seismic data velocities, Opara (2011) showed that overpressures are frequent, in particular in the deepest layers (up to 10 km deep). In these layers, a relationship has been observed between overpressured zones and the presence of shale diapirs and slippage structures. Ugwu and Nwankwo (2014) also reported overpressures linked to shale diapirism. According to Cobbold et al. (2009), overpressures are effectively linked to compression structures but the main cause of overpressures in Akata Fm and at the base of the Agbada Fm is due to hydrocarbon generation associated with chemical compaction. In this mechanism, hydrocarbon generation reaches the rock failure pressure, and the rupture of the cohesive grains associated with the weight of overlying sediments gives rise to a more efficient recompaction of the rock, which is lithified again by diagenesis. Multiple causes were also proposed by Caillet and Batiot (2003), Nordgård Bolås et al. (2004) or Nwozor et al. (2013) to explain the overpressures in the Niger Delta, based on the observation that compaction disequilibrium is not enough to reproduce the measured pressure profile. Besides, Meiller (2013) showed that the mechanism of smectite dehydration can contribute significantly to the generation of overpressures in the Niger Delta.

Several studies report mineralogical analyses at different depths across the Niger Delta sedimentary pile (Braide and Huff, 1986; Odigi, 1986; Oboh, 1992; Jubril et al., 1998), showing both a transformation of smectite to interstratified illite/smectite and to illite over depth. These studies show that illitisation progress is mainly limited by potassium availability and its mobility. Potassium is initially available from the seawater filling the pores as sediments are deposited and from the K-

bearing minerals (feldspars, micas). Then, carbonate cementation and overpressures are controlling potassium mobility in the sedimentary pile.

3.2. Well data from the studied area

The studied area (Figure 5) is located in the East of the Niger Delta (Nigeria) in shallow marine areas (seabed at about 20 m deep). Data were obtained from different exploration wells and mainly from the Ek-1 and Nk-1 wells that reach depths of 3750 and 4640 m, respectively. Benin Fm from the Pliocene to the present day is found over the first 1100 meters. Wells then reach the Agbada Fm of Tortonian and Messinian ages. Lithologies found are poorly consolidated sand with rare clay layers in the Benin Fm. The upper part of the Agbada Fm presents alternations of shales and sandstones. Deeper, these alternations are dominated by claystones whose layers can reach a thickness of several hundreds of meters. Shales from the deeper Akata Fm are not reached by the wells.

Several logs (gamma ray, resistivity, sonic, neutron density) of Ek-1 and Nk-1 wells describe the lithology and parameters such as the porosity and the apparent density as a function of depth (Figure 5). The correlated stratigraphic surfaces of the two wells were dated, based on regional biostratigraphic markers. These datings indicate a variation of the sedimentation rate over time, with a thickness of 3500 to 4000 m of Agbada Fm deposited over 3.5 My while a 500 to 1000 m-thickness of the superficial Benin Fm was deposited over 5.2 My.

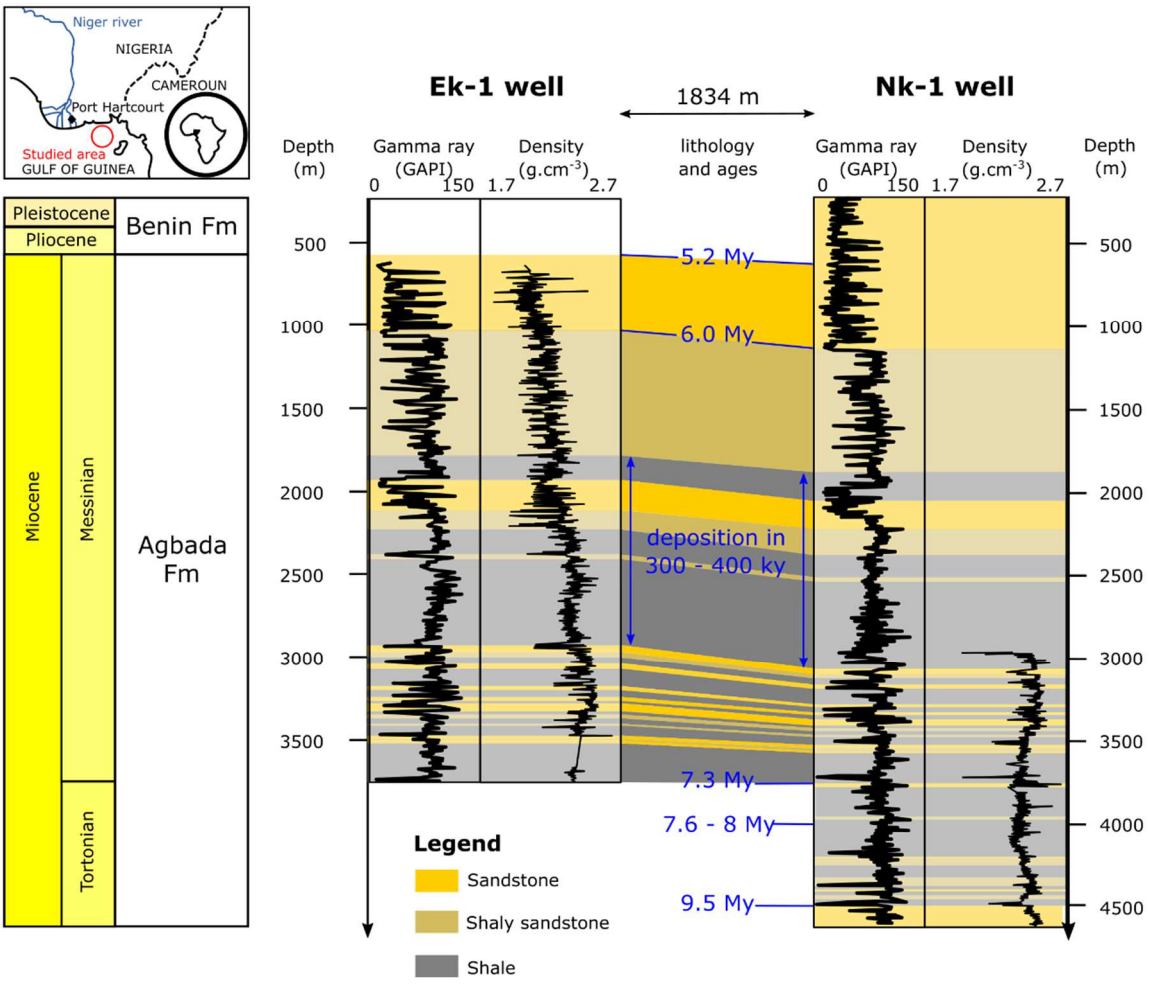

Figure 5. Interpreted log of Ek-1 and Nk-1 wells with a correlation and dating of the major stratigraphic surfaces. Location map shows the studied area in the Niger Delta.

Pore pressure was measured using the RFT method (repeat formation tester) in different wells (Ek-1, Nk-1 and Ik 1, 2, 3, 4 and 5) of the studied area in several reservoir layers. These pressure data were obtained at depths between 1420 and 4590 m (Figure 6.a). Pore pressure shows deviation from the hydrostatic pressure profile at depths greater than 2400 m, indicating an overpressure in these layers. The overpressure can reach up to 500 bar (50 MPa) in the deepest measurements. Two different overpressure regimes seem to be measured, at depths shallower or deeper than 3500 m. Between 2400 and 3500 m deep, measured pore pressures correspond to equivalent densities of 1300 to 1500 kg.m^{-3}, while below 3500 m the pore equivalent density is about 2100 kg.m^{-3}. These two different overpressure regimes can indicate different mechanisms of overpressure generation.

Temperature measurements according to depth were also performed in the different wells (Figure 6.b). The measured temperatures align with a linear geothermal gradient of 30°C.km^{-1}, typical of a passive margin context. Temperature and depth of the shale layers indicate the petroleum window is reached at the top of the overpressure zone.

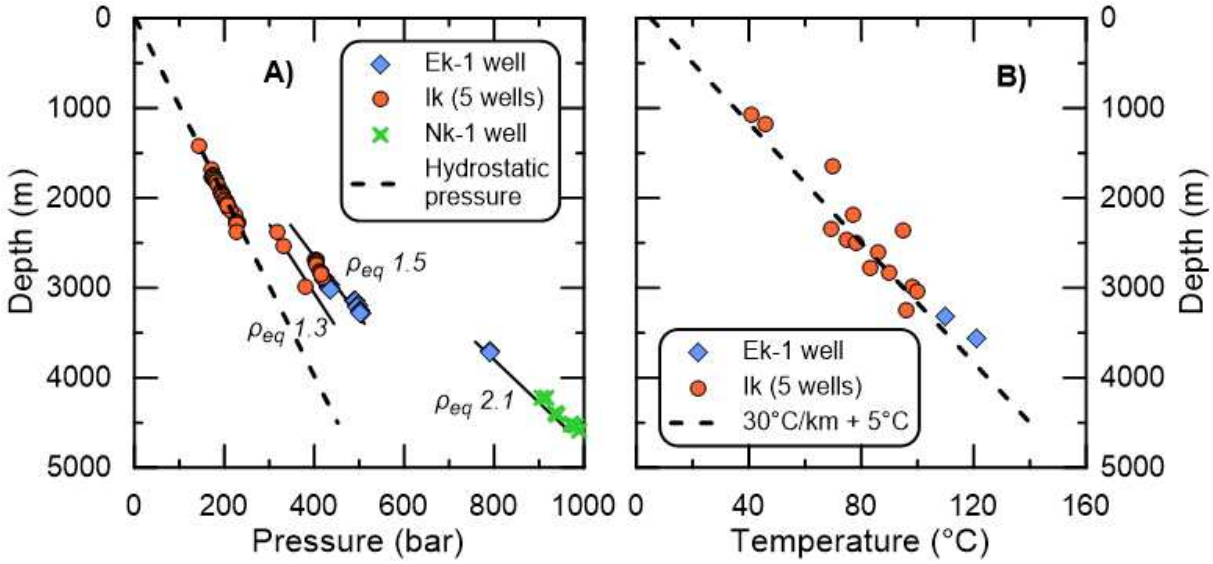

Figure 6. Measured (a) pore pressure and (b) temperature profiles in wells of the Niger Delta studied area. The pressure regimes corresponding to equivalent densities (ρ_{eq}) of 1300, 1500 and 2100 kg.m^{-3} are also shown.

3.3. Backstripping and sedimentation model

The sedimentation model aims at determining the successive layers of the sedimentary pile, evaluating the thickness of these sediments at the deposition time and estimating the sedimentation rate and its variation over time. With this aim, it is first necessary to uncompact the current sediments to obtain the thickness of the sediments at the deposition time. The backstripping approach proposed by Sclater and Christie (1980) for normally compacted sediments of different lithologies was used.

From the geological log and the recorded changes in lithology and rock properties, 45 successive lithological layers were identified in the sedimentary pile, from the seabed to the foot of Nk-1 well (Supplementary material B). Over this 4640 m-thickness, the level description in the overpressured zone (from 2400 m deep) was refined and 39 layers 7 to 407 m thick were defined. On the contrary, the upper 1040 m of the sand Benin Fm were defined as one single lithological layer. For each identified layer, the footwall and the roof depth of each lithological layer and the porosity or the apparent density were reported. Three lithology types were considered and assigned to each identified

layer: ‘shale’ for the clay rich layers; ‘shaly-sandstone’ for closely grouped alternations of claystone and sandstone layers; and ‘sandstone’ for the sandstone and sand layers.

The second step is the application of the backstripping model in itself, which consists in solving the following equation for each lithological layer:

$$z'_2 - z'_1 = z_2 - z_1 - \frac{n_0}{c}\left(e^{-c\,z_1} - e^{-c\,z_2}\right) + \frac{n_0}{c}\left(e^{-c\,z'_1} - e^{-c\,z'_2}\right) \qquad \textbf{eq. 19}$$

z_1 and z_2 are the present day roof and footwall depths (m) of the considered lithological layer, z'_1 and z'_2 are the depths at the time of deposit ($z'_1 = 0$ m) assuming that the deposit of the entire lithological layer is instantaneous. n_0 is the surface porosity which depends on the lithology (0.49 for ‘sandstone’ facies, 0.56 for ‘shaly-sandstone’ facies and 0.63 for ‘shale’ facies; Sclater and Christie (1980)). c is a compaction index dependent on the lithology (2.7 10^{-4} m^{-1} for ‘sandstone’ facies, 3.9 10^{-4} m^{-1} for ‘shaly-sandstone’ facies and 5.1 10^{-4} m^{-1} for ‘shale’ facies).

Finally, the sedimentation rate was calculated (Table 4) using the sediment thickness at the deposit time and the dating of remarkable sedimentary surfaces. Based on the evolution of the sedimentation rate over time, a period from 7.3 to 6 My can be identified when sedimentation was intense with a rate of almost 3000 $m.My^{-1}$. After 5.2 My, the sedimentation rate decreased down to about 125 $m.My^{-1}$.

Table 4. Sedimentation rate for the studied area of the Niger Delta determined for different time periods.

Period	Sedimentation rate ($m.My^{-1}$)
9.86 to 7.30 My	508.1
7.30 to 6.00 My	2868.3
6.00 to 5.20 My	429.5
5.20 My to present	124.6

3.4. Overpressure calculations for the Niger Delta case

3.4.1. Calculation scenario

The thermo-hydro-mechanical model coupled to chemical processes (SURP) previously presented was used to calculate the pore pressure evolution along the sedimentary pile of the studied area of the Niger Delta during its burial. The considered geometry is a 1D column from the seabed to the footwall

481 of the Agbada Fm. Seismic profiles indicate that the Akata Fm is located some hundreds of meters
482 below the well foots. To deal with the boundary condition between the Agbada and Akata formations
483 and without information about the inflow over time from the Akata Fm, it was decided that 500 m of
484 'shale' lithology at the foot of the modelled sedimentary pile would be included to consider the water
485 inflow from the overpressured Akata Fm. A no flow Neumann boundary condition was considered at
486 the base of these additional 500 m of shale. Additional causes of overpressure proposed for the Niger
487 Delta, such as lateral tectonic compression due to shale diapirism, were not taken into account in the
488 model. As the upper hydraulic boundary condition, hydrostatic pressure was imposed down to the
489 aquifer overlying the overpressured zone (layer shsd11, in Supplementary material B), meaning that
490 the lateral groundwater circulations occurring close to the ground surface did not require to be
491 considered.
492 The principle of the reactive model rests on the hypothesis of seawater as the initial sediment pore
493 water and an initial mineralogical assemblage that evolves as a function of temperature increase with
494 burial. In the absence of a detailed mineralogical description of the shale layers, a fictive but realistic
495 mineralogical assemblage was considered. The 'sandstone' facies was assumed to be composed only
496 of quartz. In the 'shale' and 'shaly-sandstone' lithologies, the primary mineralogical assemblage was
497 composed of montmorillonite, microcline, quartz, calcite, siderite, dolomite, pyrite and goethite. The
498 dehydration of montmorillonite took place in accordance with the thermodynamic dehydration model
499 introduced in the SURP code. Illite and kaolinite were allowed to precipitate during the simulation
500 (Supplementary material C). Water/rock reactions were controlled by thermodynamic equilibrium and
501 not by kinetics, impeding the coexistence of some aluminosilicate minerals. The assumption of a local
502 equilibrium between pore water and the surrounding reacting minerals relies mainly on the fact that
503 the interaction time was long enough to establish equilibrium conditions.
504 The simulation was run for a duration of 9.5 My, corresponding to the deposition time of the sediment
505 column drilled in the Ek-1 and Nk-1 wells. At each time step and depending on the sedimentation rate,
506 a thickness of sediment deposit and the underlying sediments already deposited are buried accordingly
507 because of the compaction model.
508

509 3.4.2. Overpressure calculation results

510 The calculated pore pressure at present day in the Niger Delta case was approximately 450 bar at 3000
511 m deep (Figure 7), corresponding to an overpressure of 150 bar at the depth of the main reservoirs. At
512 3000 m deep, good agreement was achieved between the modelled and measured fluid pressures. Two
513 pressure regimes in the overpressured zone were simulated for the profile (between 2750 and 3500 m
514 and below 4000 m), as was observed on the measured pressure profile. Nevertheless, the simulations
515 did not reproduce the deepest (< 4000 m) measured pressures. Indeed, the model does not take into
516 account the influence of the deep Akata shale on overpressures and this influence seems to explain the
517 remaining 100 to 200 bar required to match the present day pressure profile.

518 According to the calculations, smectite dehydration was inducing an excess pressure of about 50 bar
519 on the present day pressure profile at 3000 m deep compared to the simulation accounting only for
520 compaction and thermal effects (Figure 7). The release of water due to smectite dehydration and
521 illitisation can explain a third of the overpressure. A simulation performed accounting for smectite
522 dehydration but without smectite illitisation gave a pressure 5 bar lower than the pressure calculated
523 considering both smectite dehydration and illitisation (in addition to the thermo-mechanical
524 phenomena) at 3000 m deep, and 10 bar lower at the bottom of the modelled sedimentary column.
525 Smectite dehydration thus appears as the main source of water released by smectite. The initial amount
526 of smectite in the sediment also has an influence on the generated overpressure. For example, by
527 dividing the amount of Na-montmorillonite by two (15 $\%_{vol}$ for 'shale' facies and 7.5$\%_{vol}$ for 'shaly-
528 sandstone' facies), the calculated overpressure at the present day is 20 bar higher than without the
529 release of water by smectite at 3000 m deep, corresponding to 10 to 15 % of the total overpressure.

530 Figure 8 shows the evolution of the calculated overpressure over time since the beginning of the
531 sediment deposition and as a function of depth. The period with a high sedimentation rate is well
532 identified in this figure where major burial and sediment accumulation was simulated. It resulted in a
533 build-up of the overpressure, which reached values of 500 bar at the bottom of the sedimentary pile
534 and 400 bar at 3000 m deep during this high sedimentation rate period. This pressure build-up is
535 related to the compaction disequilibrium that occurred during this period with the fluids stressed
536 within the porosity, the increase of fluid volume with temperature (aquathermal expansion) and the

release of water from clay minerals that was more efficient with the rapid increases in temperature and pressure. When only compaction and thermal effects were considered, the maximal overpressure reached within this period was 350 bar at 3000 m and 500 bar at the bottom of the modelled column. The overpressure was then simulated to dissipate after the Pliocene, when the sedimentation rate noticeably decreased. Compaction and water release by smectite were less efficient during this final period, allowing the pressure to decrease depending on the hydraulic parameters acquired during burial.

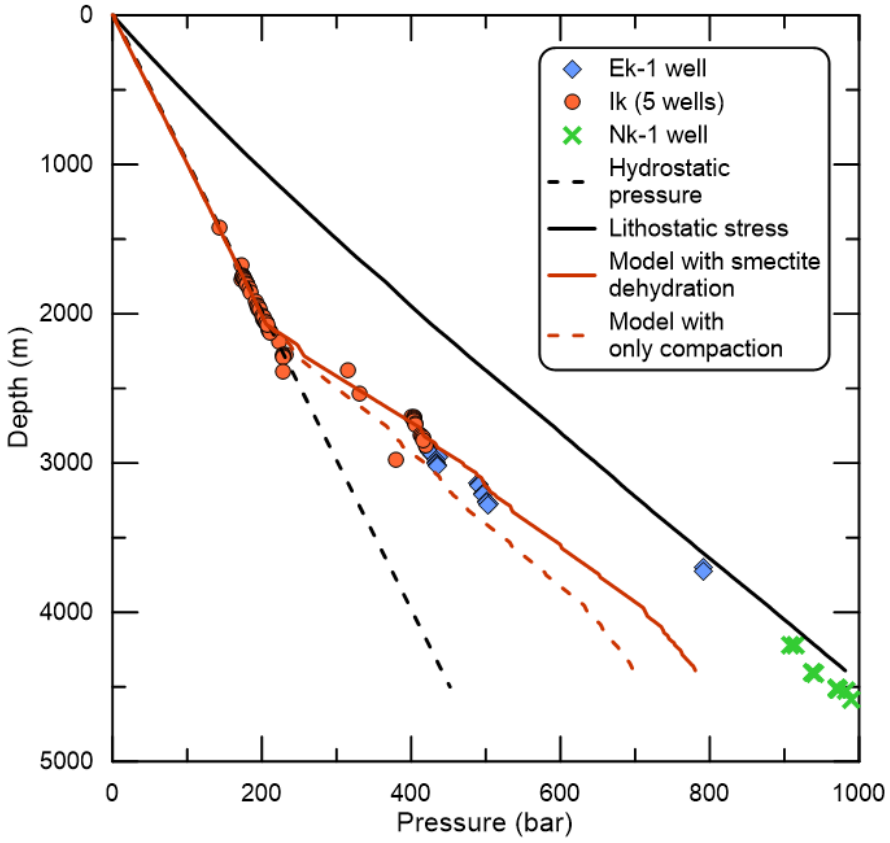

Figure 7. Present day modelled and observed pore pressure profiles in the Niger Delta area considered for SURP application. By comparing the two models which may or may not account for the chemical processes, the effect of the release of water by smectite dehydration and illitisation on the abnormal fluid pressure can be evaluated.

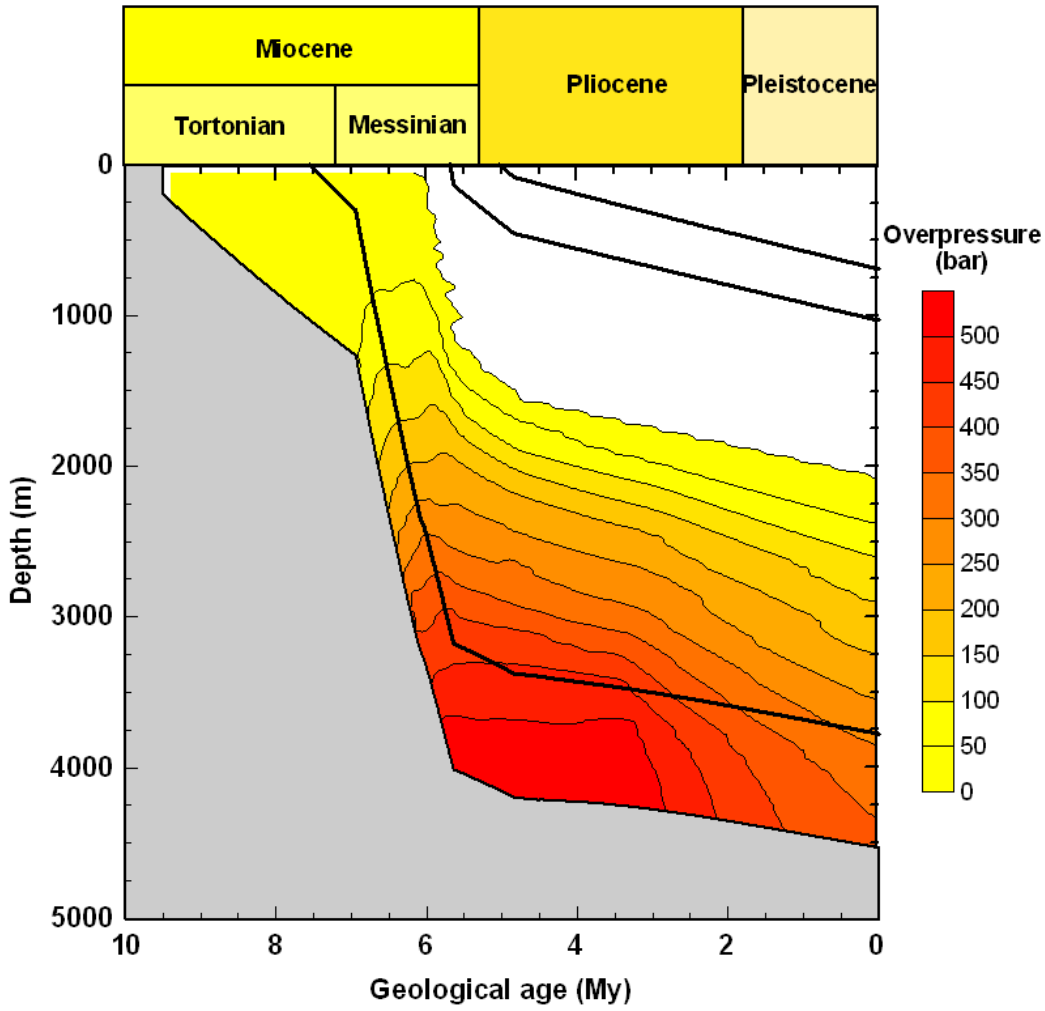

Figure 8. Simulated overpressure evolution as a function of geological age and depth in the Niger Delta. The grey area corresponds to a zone outside of the model. The simulation accounts for the clay dehydration and smectite-to-illite transformation processes.

3.4.3. Compaction model results

After 9.5 My of simulation, the model gave a sediment thickness of 4428 m to be compared to the 4640 m of the well log. This sediment thickness was achieved after the initial backstripping calculation followed by the forward modelling of the deposition and burial of the sediments for overpressure evaluation. The main difference in thickness between the model and the field resided in the superior sandstone layer that was not uncompacted during backstripping and was modelled at a thickness of 956 m compared to the well thickness of 1040 m. Moreover, compaction was slightly overestimated for 'shale' facies (≈ 5%) and underestimated for 'sandstone' facies (≈ 2%).

The porosity decreased because of compaction for each lithology (Figure 9.a), with porosities lower than 15% below 3000 m for the 'shale' facies at present day. Hydraulic permeability (Figure 9.b) and

other porosity-dependent hydro-mechanical parameters evolved as the porosity decreased. The permeability reached values of about 10^{-21} m² for the 'shale' lithology at depth, forming an efficient caprock to limit the dissipation of the overpressure built up during the maximal burial period, so that the overpressure is still monitored at present day. Permeability for 'shaly-sandstone' facies was simulated between 10^{-19} and 10^{-20} m² and permeability for 'sandstone' remained constant at 10^{-16} m².

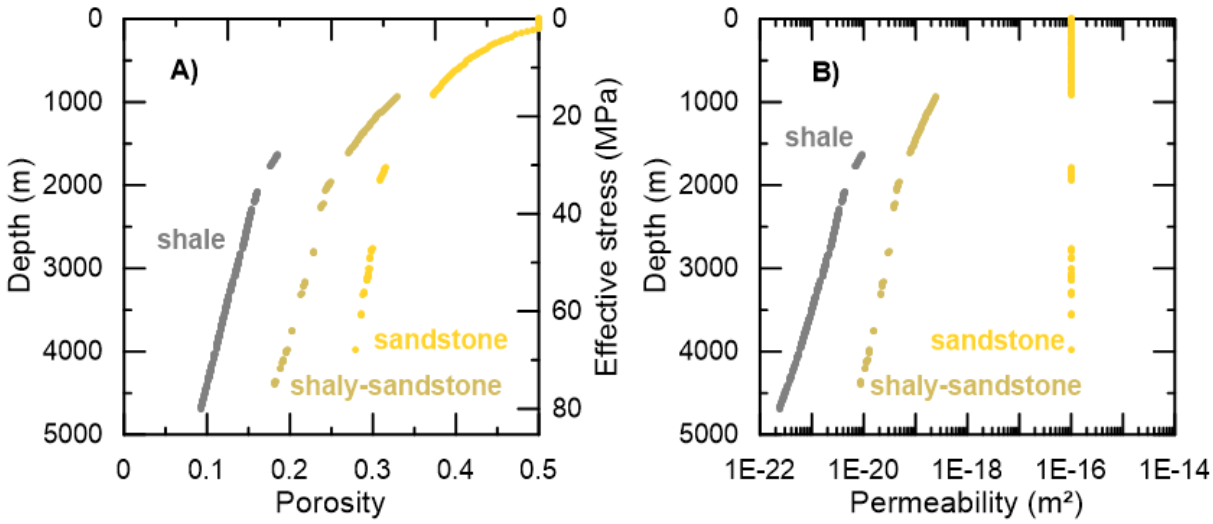

Figure 9. Simulated present day (a) porosity and (b) permeability profiles. The 3 lithological facies used in the model are distinguished by their colour, showing the difference in compaction trends for each facies.

3.4.4. Mineralogical evolution results

The mineralogical evolution can be inferred by the present day mineralogical profile (Figure 10), at the end of the simulation. The 'shale' and 'shaly-sandstone' facies are identified in the profile by the differences in mineral content. Mineralogical composition evolves with depth because temperature is the main reactivity factor of control. Hydrated Na-montmorillonite content is observed to diminish with depth while anhydrous Na-montmorillonite content increases, revealing the dehydration of Na-montmorillonite. The transition from hydrated Na-montmorillonite with two layers of water to one layer of water is located at about 3070 m (96 °C and 485 bar) and corresponds to a sudden release of water. The transition from three layers of water to two layers is not observed on the present day profile because this transition occurred at about 850 m (30°C), at a depth where the 'sandstone' lithology is currently found. Hydrated montmorillonite content also concomitantly decreases at the depth where

illite forms (about 2500 m). Dissolution of microcline also accompanied this illitisation on the profile, acting as a source of K^+ that stabilizes illite. The modelled mineralogical evolution is thus consistent with the expected smectite-to-illite reactive pathway and smectite dehydration process. The evolution of the calculated CO_2 partial pressure with increasing temperature (Figure 10.B) is in line with the pCO_2 usually measured in sedimentary basins (Coudrain-Ribstein et al., 1998). Since the pCO_2 is calculated from an equilibrium between the different involved minerals and the pore water for evolving temperature and pressure conditions, the agreement between calculated and measured pCO_2 is an another indication of the consistence of the mineralogical assemblage selection.

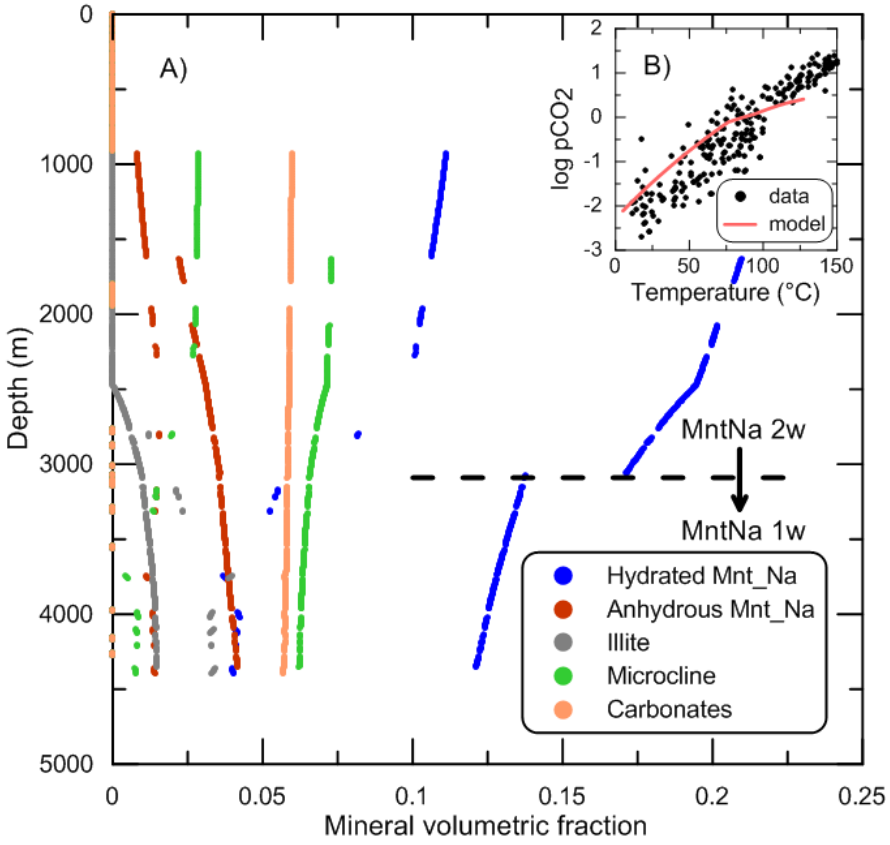

Figure 10. A) Simulated present day mineralogical profile. Hydrated Mnt_Na: 3w, 2w or 1w Na-montmorillonite; Anhydrous Mnt_Na: anhydrous Na-Montmorillonite; Carbonates: sum of calcite, dolomite and siderite. B) Comparison of calculated pCO_2 with pCO_2 data from sedimentary formations (Coudrain-Ribstein et al., 1998). *With the exception of the Mnt_Na 2w to Mnt_Na 1w hydrated smectite transition, the discontinuities in mineral content that are seen in the profile are linked to the distribution of lithological facies with depth.*

4. Discussion

A thermo-hydro-mechanical model coupled with an advanced thermodynamic model for smectite dehydration has been developed to calculate overpressures during the burial of a sedimentary pile.

Named SURP, this overpressure calculation code accounts for mechanical compaction, thermal effects and water release by smectite. Hence, the effect of pressure and temperature on the smectite dehydration process can be taken into account and the water released is considered in the pressure calculation. This coupling clearly goes beyond the previous models that considered smectite dehydration through an approximated evaluation of a source term in the overpressure calculation (Audet, 1995; Wangen, 2001) or considered smectite dehydration properly but without a feedback on pressure (Colten-Bradley, 1987; Meiller, 2013).

The SURP code was applied to the case study of the Niger Delta, formed of thick shale layers. Depending on the clay content, smectite dehydration was simulated to be the cause of 10 to 30 % of the present day overpressure in the main reservoirs, in addition to the compaction disequilibrium. The overpressure built-up during the Messinian is still high (about 200 bar at 3000 m deep) despite its dissipation. Water release by illitisation of smectite has much less influence on the pressure profile than smectite dehydration.

Although dependent on the smectite content in the sedimentary pile, the geological scenario and the hydraulic conditions and parameters, the calculated contribution of smectite dehydration to overpressure is in the range of previously estimated contributions. Audet (1995) calculated that dehydration can increase overpressuring by about 30 % provided that the sediments are relatively impermeable and that sufficient water is released. Also in a theoretical scenario, Wangen (2001) calculated a contribution of smectite dehydration in the same range, of about ¼ to ⅓ of the overpressure. The examples of quantification of the contribution of smectite dehydration to overpressures are few in the literature since the release of water is often considered as only one contributor amongst other unloading processes that decrease the effective stress without modifying the porosity. In the North Sea Viking Graben (Nordgård Bolås et al., 2004) and Central Graben (Kooi, 1997), smectite dehydration is discussed as a potential additional overpressuring mechanism as compaction disequilibrium alone is not sufficient to explain the measured overpressure, and other possible mechanisms were ruled out. In the Gulf of Mexico, offshore Louisiana, Gordon and Flemings (1998) simulated that, depending on the elastic or inelastic compaction model considered, clay dehydration can provide up to 20 % of the overpressure. Clay dehydration is also discussed in the Gulf

632 of Mexico as a possible source of overpressure by Bruce (1984) and Shaw and Primmer (1989), based
633 on the observation that the onset of the overpressure coincides with the smectite-to-illite
634 transformation. In the Western Foothills of Taiwan, Tanikawa et al. (2008) performed overpressure
635 calculations suggesting that clay dehydration is a secondary mechanism generating overpressures,
636 complementary to compaction disequilibrium and more significant than hydrocarbon generation. In
637 the Taiwan case, it is estimated that at the maximum pressure build-up, clay dehydration can double
638 the calculated overpressure compared to cases in which only compaction and thermal expansion are
639 taken into account. Overpressure nevertheless dissipated then and a basal fluid flux was necessary to
640 explain the present day pressure profile.
641 Clay dehydration is often ruled out as a mechanism contributing to overpressure because the volume
642 increase due to the water produced by smectite dehydration was estimated at only 1.4 % below a depth
643 of 1 km, which is the depth at which overpressures are observed to develop (Swarbrick and Osborne,
644 1998). Our results are at the opposite: when clay dehydration is integrated in forward modelling of
645 overpressure, the different examples, including ours, suggest that the release of water by smectite
646 dehydration or by illitisation can contribute to the pressure profile as an important additional
647 contributor to compaction disequilibrium.
648 Although able to consider each process that can contribute to the overpressure build-up and dissipation
649 calculations individually, the forward modelling approach we considered presents limitations inherent
650 to every hydraulic and water/rock interaction model. The two key factors in a hydraulic model are the
651 boundary conditions and their evolution over time, and the hydraulic conductivity and its dependence
652 on compaction and porosity reduction (Person et al., 1996; Bjørlykke et al., 2010). The hydraulic
653 boundary condition at the base of the sedimentary pile is generally unknown and a simple and
654 idealized boundary condition is often considered. A no flow basal boundary condition is a convenient
655 approach but is evidently complicated to verify. In the case of the Niger Delta, we had no information
656 about an inflow at 5000 m deep, at the bottom of the sedimentary pile of our model. Seismic data
657 indicated an apparent density in line with the deepest pressure measurements. The hydraulic and
658 hydro-mechanical parameters used in the simulation have a high influence on the flow and pressure
659 regime in the modelled sedimentary pile. In our study, we used porosity-dependent empirical

660 relationships to determine these parameters, calibrated on various sets of experimental data
661 (Supplementary material A). The scattering of the data around the empirical relationships illustrates
662 the variability of these parameters. When data from the studied site are available, the empirical
663 relationships can be calibrated on these data. However, data scattering around the law may be
664 unavoidable, which may affect the robustness of the law.
665 Limitations of the water/rock interaction model rely on the fact that it is necessary to know the pore
666 water composition and its evolution, and that mineralogical and petrographical data are necessary for
667 good constraining of the interaction model (Person et al., 1996). For instance, the depths of the
668 smectite dehydration reactions and the smectite-to-illite transformation may vary significantly
669 according to the chemical composition of the clay phases or the variation of the thermodynamic
670 parameters within their error margins. Based on this knowledge and on the reasonable assumptions
671 that seawater was trapped in the sediment porosity and that the initial mineralogical assemblage
672 corresponded to a clay-rich sediment, our model has been able to simulate the expected illitisation of
673 smectite, accompanied by microcline dissolution. Reactive transport models have already been applied
674 to diagenesis modelling (e.g. Le Gallo et al., 1998), giving valuable simulations of mineral evolution
675 in reservoirs.
676

677 ## 5. Conclusion

678 In this study, we developed the first overpressure calculation code including a thermodynamic
679 description of clay dehydration. We draw upon recent advances in clay thermodynamics and in
680 numerical modelling of solid solutions to precisely calculate the quantity of water that can be expulsed
681 within the porosity of clay formations during smectite dehydration and illitisation processes. Hence,
682 the SURP code considers water flow, compaction, temperature increase and smectite dehydration and
683 illitisation, with a reciprocal effect, during the burial of a sedimentary pile.
684 The application of the SURP code to the Niger Delta case study evidenced that 10 to 30 % of the
685 present day overpressure in the main reservoirs can be explained by smectite dehydration. Up to now,
686 relatively few cases of overpressures generated by smectite dehydration have been reported and this
687 mechanism is often not considered because of the lack of a tool able to calculate its effect. With a code

688 such as SURP, it is possible to evaluate the influence of smectite dehydration on overpressure build-up
689 in passive margins, but also in compressive domains.
690 One of the future prospects of this work should be the introduction of this type of calculation in 2D or
691 3D basin modelling in order to better constrain boundary conditions and investigate how the water
692 production by clay formations can contribute to the general fluid flow in the basin. Another prospect
693 should be the improvement of the capabilities of the SURP code in simulating coupled mineralogical
694 and hydro-mechanical evolution as a diagenesis code that can differentiate the porosity evolution due
695 to mechanical compaction and diagenesis.
696

697 ## Acknowledgments

698 This work was funded by TOTAL S.A. The authors are grateful to two anonymous reviewers for their
699 helpful comments and to Friedemann Baur associate Editor for handling the manuscript.
700

701 ## References

702 Altaner, S.P., 1989. Calculation of K diffusional rates in bentonite beds. Geochimica et Cosmochimica
703 Acta 53, 923–931.
704 Altaner, S.P., Ylagan, R.F., 1997. Comparison of structural models of mixed-layer illite/smectite and
705 reaction mechanisms of smectite illitization. Clays and Clay Minerals 45, 517–533.
706 Audet, D.M., 1995. Mathematical modelling of gravitational compaction and clay dehydration in thick
707 sediment layers. Geophysical Journal International 122, 283–298.
708 Bjørlykke, K., Jahren, J., Aagaard, P., Fisher, Q., 2010. Role of effective permeability distribution in
709 estimating overpressure using basin modelling. Marine and Petroleum Geology 27, 1684–
710 1691.
711 Blanc, P., Lassin, A., Piantone, P., Azaroual, M., Jacquemet, N., Fabbri, A., Gaucher, E.C., 2012.
712 Thermoddem: A geochemical database focused on low temperature water/rock interactions
713 and waste materials. Applied Geochemistry 27, 2107–2116.
714 Blanc, P., Vieillard, P., Gailhanou, H., Gaboreau, S., Gaucher, E., Fialips, C. I., Giffaut, E., 2015. A
715 generalized model for predicting the thermodynamic properties of clay minerals. American
716 Journal of Science 315, 734–780.
717 Braide, S.P., Huff, W.D., 1986. Clay mineral variation in Tertiary sediments from the eastern flank of
718 the Niger Delta. Clay Minerals 21, 211–224.
719 Bruce, C.H., 1984. Smectite dehydration; its relation to structural development and hydrocarbon
720 accumulation in northern Gulf of Mexico basin. AAPG Bulletin 68, 673–683.
721 Burland, J.B., 1990. On the compressibility and shear strength of natural clays. Géotechnique 40, 329–
722 378.
723 Burrus, J., 1998. Overpressure models for clastic rocks, their relation to hydrocarbon expulsion: a
724 critical reevaluation, in: Law, B.E., Ulmishek, G.F., Slavin, V.I. (Eds.), AbnormalPressures
725 Hydrocarbon Environments, AAPGMemoir. AAPG, pp. 35–64.
726 Burst, J.F., 1969. Diagenesis of Gulf Coast clayey sediments and its possible relation to petroleum
727 migration. AAPG Bulletin 53, 73–93.
728 Caillet, G., Batiot, S., 2003. 2D modelling of hydrocarbon migration along and across growth faults:
729 an example from Nigeria. Petroleum Geoscience 9, 113–124.

730 Charlton, S.R., Parkhurst, D.L., 2011. Modules based on the geochemical model PHREEQC for use in
731 scripting and programming languages. Computers & Geosciences 37, 1653–1663.
732 Chukwu, G.A., 1991. The Niger Delta complex basin: stratigraphy, structure and hydrocarbon
733 potential. Journal of Petroleum Geology 14, 211–220.
734 Cobbold, P.R., Clarke, B.J., Loseth, H., 2009. Structural consequences of fluid overpressure and
735 seepage forces in the outer thrust belt of the Niger Delta. Petroleum Geosciences 15, 3–15.
736 Colten-Bradley, V.A., 1987. Role of pressure in smectite dehydration; effects on geopressure and
737 smectite-to-illite transformation. AAPG Bulletin 71, 1414–1427.
738 Coudrain-Ribstein, A., Gouze, P., Marsily, G. de, 1998. Temperature-carbon dioxide partial pressure
739 trends in confined aquifers. Chemical Geology 145, 73–89.
740 Cuadros, J., 2006. Modeling of smectite illitization in burial diagenesis environments. Geochimica et
741 Cosmochimica Acta 70, 4181–4195.
742 De Marsily, G., 1986. Quantitative Hydrogeology. Academic Press.
743 Dubacq, B., Vidal, O., De Andrade, V., 2010. Dehydration of dioctahedral aluminous phyllosilicates:
744 thermodynamic modelling and implications for thermobarometric estimates. Contributions to
745 Mineralogy and Petrology 159, 159–174.
746 Ferrage, E., Lanson, B., Sakharov, B.A., Drits, V.A., 2005. Investigation of smectite hydration
747 properties by modeling experimental X-ray diffraction patterns: Part I. Montmorillonite
748 hydration properties. American Mineralogist 90, 1358–1374.
749 Gordon, D.S., Flemings, P.B., 1998. Generation of overpressure and compaction-driven fluid flow in a
750 Plio-Pleistocene growth-faulted basin, Eugene Island 330, offshore Louisiana. Basin Research
751 10, 177–196.
752 Ingebritsen, S., Sanford, W., Neuzil, C., 2006. Groundwater in geologic processes. Cambridge
753 University Press.
754 Inoue, A., Kohyama, N., Watanabe, T., 1987. Chemical and morphological evidence for the
755 conversion of smectite to illite. Clays and Clay Minerals 35, 111–120.
756 Jubril, M.A., Shaw, H.F., Fallick, A.E., 1998. Stable isotope and geochemical evidence of formation
757 pore fluid evolution during diagenesis of Tertiary sandstones and mudrocks of the Niger Delta.
758 Journal of African Earth Science 27, 417–435.
759 Kooi, H., 1997. Insufficiency of compaction disequilibrium as the sole cause of high pore fluid
760 pressures in pre-Cenozoic sediments. Basin Research 9, 227–241.
761 Lambe, T.W., Whitman, R.V., 1979. Soil mechanics, Series in soil engineering. Wiley.
762 Lanson, B., Sakharov, B.A., Claret, F., Drits, V.A., 2009. Diagenetic smectite-to-illite transition in
763 clay-rich sediments: A reappraisal of X-ray diffraction results using the multi-specimen
764 method. American Journal of Science 309, 476–516.
765 Le Gallo, Y., Bildstein, O., Brosse, E., 1998. Coupled reaction-flow modeling of diagenetic changes in
766 reservoir permeability, porosity and mineral compositions. Journal of Hydrology 209, 366–
767 388.
768 Meiller, C., 2013. Etude cristallochimique de solutions solides de minéraux argileux. Impact de la
769 déshydratation des smectites sur les surpressions dans les bassins sédimentaires.
770 Meunier, A., Velde, B., 1989. Solid solution in I/S mixed-layer minerals and illite. American
771 Mineralogist 74, 1106–1112.
772 Neuzil, C.E., 1995. Abnormal pressures as hydrodynamic phenomena. American Journal of Science
773 295, 742–786.
774 Nordgård Bolås, H.M., Hermanrud, C., Teige, G.M., 2004. Origin of overpressures in shales:
775 Constraints from basin modeling. AAPG bulletin 88, 193–211.
776 Nwozor, K.K., Omudu, M.L., Ozumba, B.M., Egbuachor, C.J., Onwuemesi, A.G., Anike, O.L., 2013.
777 Quantitative evidence of secondary mechanisms of overpressure generation: insights from
778 parts of onshore Niger Delta, Nigeria. Petroleum Technology Development Journal 3, 64–83.
779 Nygård, R., Gutierrez, M., Gautam, R., Høeg, K., 2004. Compaction behavior of argillaceous
780 sediments as function of diagenesis. Marine and Petroleum Geology 21, 349–362.
781 Oboh, F.E., 1992. Middle Miocene palaeoenvironments of the Niger Delta. Palaeogeography,
782 Palaecclimatology, Palaeoecology 92, 55–84.

783 Odigi, M.I., 1986. Mineralogical and geochemical studies of Tertiary sediments from the eastern Niger
784 Delta and their relationship to petroleum occurence. Journal of Petroleum Geology 10, 101–
785 114.
786 Opara, A., 2011. Estimation of multiple sources of overpressures using vertical effective stress
787 approach: case study of the Niger Delta, Nigeria. Petroleum & Coal 53.
788 Owolabi, O.O., Okpobiri, G.A., Obomanu, I.A., 1990. Prediction of abnormal pressure in the Niger
789 Delta Basin using well logs. SPE 021575, 1–15.
790 Parkhurst, D.L., Appelo, C.A.J., 2013. Description of input and examples for PHREEQC Version 3–a
791 computer program for speciation, batch-reaction, one-dimensional transport, and inverse
792 geochemical calculations. U.S. Geological Survey.
793 Perry, E.A., Hower, J., 1970. Burial diagenesis in Gulf Coast pelitic sediments. Clays and Clay
794 Minerals 18, 165–177.
795 Person, M., Raffensperger, J.P., Ge, S., Garven, G., 1996. Basin-scale hydrogeologic modeling.
796 Reviews of Geophysics 34, 61–87.
797 Pytte, A.M., Reynolds, R.C., 1989. The thermal transformation of smectite to illite, in: Naeser, T.H.
798 N.D. McCulloh (Ed.), The Thermal History of Sedimentary Basins. Springer, New York, pp.
799 133–140.
800 Ransom, B., Helgeson, H.C., 1994. A chemical and thermodynamic model of aluminous dioctahedral
801 2:1 layer clay minerals in diagenetic processes; regular solution representation of interlayer
802 dehydration in smectite. American Journal of Science 294, 449–484.
803 Saffer, D.M., McKiernan, A.W., 2009. Evaluation of in situ smectite dehydration as a pore water
804 freshening mechanism in the Nankai Trough, offshore southwest Japan. Geochemistry,
805 Geophysics, Geosystems 10.
806 Sclater, J.G., Christie, P.A.F., 1980. Continental stretching: An explanation of the Post-Mid-
807 Cretaceous subsidence of the central North Sea Basin. Journal of Geophysical Research: Solid
808 Earth 85, 3711–3739.
809 Shaw, H.F., Primmer, T.J., 1989. Diagenesis in shales from a partly overpressured sequence in the
810 Gulf Coast, Texas, USA. Marine and Petroleum Geology 6, 121–128.
811 Srodon, J., Zeelmaekers, E., Derkowski, A., 2009. The charge of component layers of illite-smectite in
812 bentonites and the nature of end-member illite. Clays and Clay Minerals 57, 649–671.
813 Swarbrick, R.E., Osborne, M.J., 1998. Mechanisms that Generate Abnormal Pressures: an Overview,
814 in: Law, B.E., Ulmishek, G.F., Slavin, V.I. (Eds.), AbnormalPressures Hydrocarbon
815 Environments, AAPGMemoir. AAPG, pp. 13–34.
816 Tanikawa, W., Shimamoto, T., Wey, S., Lin, C., Lai, W., 2008. Stratigraphic variation of transport
817 properties and overpressure development in the Western Foothills, Taiwan. Journal of
818 Geophysical Research: Solid Earth 113.
819 Tremosa, J., Gonçalvès, J., Matray, J.M., 2012. Natural conditions for more limited osmotic abnormal
820 fluid pressures in sedimentary basins. Water Resources Research 48.
821 Ugwu, S.A., Nwankwo, C.N., 2014. Integrated approach to geopressure detection in the X-field,
822 Onshore Niger Delta. Journal of Petroleum Exploration and Production Technology 4, 215–
823 231.
824 Van Der Kamp, G., Gale, J.E., 1983. Theory of earth tide and barometric effects in porous formations
825 with compressible grains. Water Resources Research 19, 538–544.
826 Velde, B., Brusewitz, A.M., 1986. Compositional variation in component layers in natural
827 illite/smectite. Clays and Clay Minerals 34, 651–657.
828 Velde, B., Vasseur, G., 1992. Estimation of the diagenetic smectite to illite transformation in time-
829 temperature space. American Mineralogist 77, 967–976.
830 Vidal, O., Dubacq, B., 2009. Thermodynamic modelling of clay dehydration, stability and
831 compositional evolution with temperature, pressure and H_2O activity. Geochimica et
832 Cosmochimica Acta 73, 6544–6564.
833 Wangen, M., 2001. A quantitative comparison of some mechanisms generating overpressure in
834 sedimentary basins. Tectonophysics 334, 211–234.
835 Weaver, C.E., 1959. Possible uses of clay minerals in the search for oil. Clays and Clay Minerals 8,
836 214–227.
837 Whiteman, A., 1982. Nigeria: its petroleum geology, resources and potential. Graham & Trotman.